Letter

Translating nano-Hertz gravitational wave background into primordial perturbations taking account of the cosmological QCD phase transition

Katsuya T. Abe[1,*] and Yuichiro Tada[2,3,†]

[1]*Center for Frontier Science, Chiba University, 1-33 Yayoi-cho, Inage-ku, Chiba 263-8522, Japan*
[2]*Institute for Advanced Research, Nagoya University, Furo-cho Chikusa-ku, Nagoya 464-8601, Japan*
[3]*Department of Physics, Nagoya University, Furo-cho Chikusa-ku, Nagoya 464-8602, Japan*

(Received 7 August 2023; accepted 7 November 2023; published 30 November 2023)

The evidence of the nano-Hertz stochastic gravitational wave (GW) background is reported by multiple pulsar timing array collaborations. While a prominent candidate of the origin is astrophysical from supermassive black hole binaries, alternative models involving GWs induced by primordial curvature perturbations can explain the inferred GW spectrum. Serendipitously, the nano-Hertz range coincides with the Hubble scale during the cosmological quantum chromodynamics (QCD) phase transition. The influence of the QCD phase transition can modify the spectrum of induced GWs within the nano-Hertz frequency range, necessitating careful analysis. We estimate GWs induced by power-law power spectra of primordial curvature perturbations taking account of the QCD phase transition. Then we translate the implication of the NANOGrav data into the constraint on the power spectrum of the primordial curvature perturbation, which suggests one would underestimate the amplitude by about 25% and the spectral index by up to 10% if neglecting the QCD effect.

DOI: 10.1103/PhysRevD.108.L101304

Introduction. The evidence of the stochastic GW background in the nano-Hertz range is reported by the NANOGrav [1], European Pulsar Timing Array [2], Parkes Pulsar Timing Array [3], and Chinese Pulsar Timing Array [4]. The inferred spectrum is consistent with the astrophysical expectation from supermassive black hole binaries, but it can be also explained by some primordial origin [5,6] represented by the induced GW due to large primordial curvature perturbations [7–13] (see, e.g., Ref. [14] for the induced-GW interpretation of the NANOGrav 11-yr data). In particular, GWs with the observed amplitude and frequency range would correspond to sizable enough perturbations which can cause primordial black holes (PBHs) of the stellar mass [15–19] (see also the recent review article [20]). Such stellar mass PBHs can explain some fraction of black hole binaries found by merger GWs in the LIGO-Virgo-KAGRA collaboration [21–24]. Large primordial perturbations themselves are viewed as important information on the detailed mechanism of cosmic inflation.

Serendipitously, the nano-Hertz range coincides with the Hubble scale during the cosmological QCD phase transition. There, the equation-of-state parameter $w = p/\rho$ and the sound speed (squared) $c_s^2 = \partial p/\partial\rho$, where ρ and p are energy density and pressure, slightly reduce from the exact radiation value, $1/3$, (see Fig. 1) and hence the compaction of the density perturbation and also the dilution of the induced GW are affected [25]. In fact, the resultant GW spectrum shows a sharp drop in this range even if the input primordial curvature perturbation is exactly scale-invariant (see Fig. 2). Hence, a naive estimate without the QCD effect can miss the true implication. In this paper, given input (compact) power-law power spectra of curvature perturbations, we numerically calculate the resultant spectra of the induced GWs with the QCD effect in the nano-Hertz range and derive fitting formulae for their amplitude and scale dependence with respect to the input parameters. Making use of these formulae, specifically, the implication of the NANOGrav data (see Fig. 3) is translated into the constraint on the power spectrum of the primordial curvature perturbation.[1] Throughout this paper, we adopt the natural unit $c = \hbar = 1$.

Induced gravitational waves during the QCD phase transition. We briefly review Ref. [25] for GW induction during the QCD phase transition. Let us first specify the background dynamics. The temperature dependence of the effective degrees of freedom for energy density, g_*, and

*kabe@chiba-u.jp
†tada.yuichiro.y8@f.mail.nagoya-u.ac.jp

[1]See Refs. [26–29] for the implication on the PBH and induced GW (without the QCD effect) of the latest NANOGrav data. See also Ref. [30] for a discussion of the QCD effect (only on w) on the primordial GW in general contexts in nano-Hertz frequency ranges.

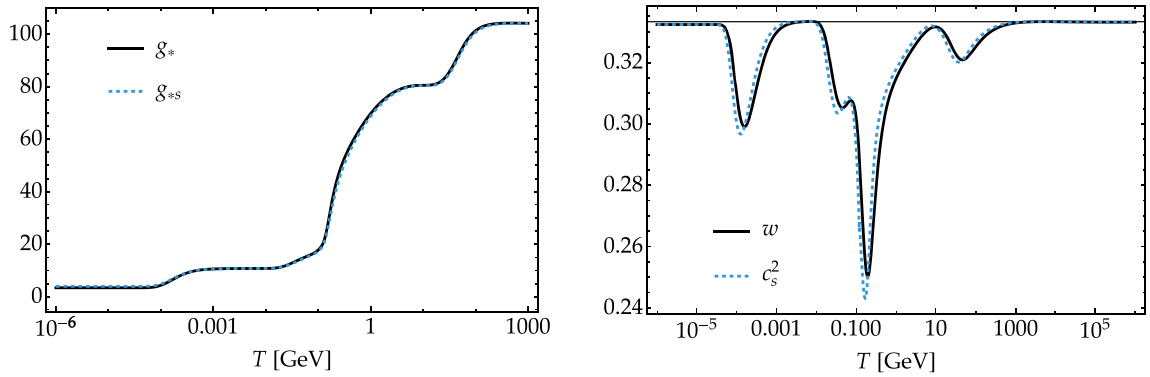

FIG. 1. Left: the temperature dependence of the effective degrees of freedom for energy density, g_* (black), and entropy density, g_{*s} (light-blue dashed). We adopt the fitting formula given in Appendix C of Ref. [31] throughout this paper. Right: corresponding equation-of-state parameter w (black) and the sound speed squared c_s^2 (light-blue dashed) (1). The horizontal line $w = c_s^2 = 1/3$ is the value of the exact radiation fluid.

entropy density, g_{*s}, of the QCD plasma has been extensively studied both in analytic and numerical ways. Saikawa and Shirai unified these results in the form of the fitting function (see Appendix C of Ref. [31]), which is plotted in the left panel of Fig. 1. These effective degrees of freedom are related to w and c_s^2 by

$$w(T) = \frac{4g_{*s}(T)}{3g_*(T)} - 1,$$
$$c_s^2(T) = \frac{4(g'_{*s}(T)T + 4g_{*s}(T))}{3(g'_*(T)T + 4g_*(T))} - 1, \tag{1}$$

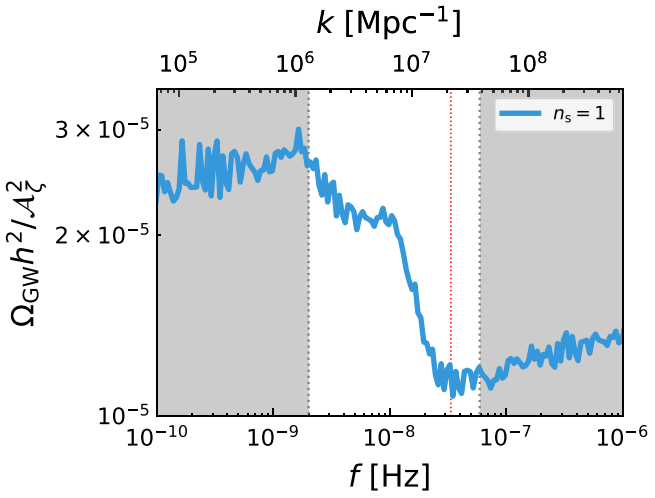

FIG. 2. The spectral shape of the current energy density of GWs induced by the scale-invariant spectrum (light blue), whose amplitude is normalized by A_ζ^2. The GW frequency f is related with its wave number k by $f = k/(2\pi)$. The noisy feature on the induced spectrum is merely caused by the numerical error. The unshaded region shows the NANOGrav's sensitivity range $f = 2$–59 nHz and the red dotted line indicates the pivot scale $f_{\mathrm{yr}^{-1}} = 1\ \mathrm{yr}^{-1} \simeq 31.7$ nHz of the analysis.

which are shown in the right panel of Fig. 1. Once their temperature dependence is fixed, the time evolution of the temperature of the universe (and hence the evolution of all background parameters) can be calculated through the continuity equation, the Friedmann equation, and the definition of g_*:

$$\frac{\mathrm{d}\rho}{\mathrm{d}\eta} = -3(1+w)\mathcal{H}\rho,$$
$$3M_{\mathrm{Pl}}^2\mathcal{H}^2 = a^2\rho, \qquad \rho(T) = \frac{\pi^2}{30}g_*(T)T^4. \tag{2}$$

a is the scale factor, $\eta = \int a^{-1}\mathrm{d}t$ is the conformal time, $\mathcal{H} = \partial_\eta \ln a$ is the conformal Hubble parameter, and $M_{\mathrm{Pl}} = 1/\sqrt{8\pi G}$ is the reduced Planck mass.

Perturbations evolve along this background. The (Fourier-space) gravitational potential $\hat{\Phi}_{\mathbf{k}}(\eta)$ in the Newton gauge follows the Bardeen equation,

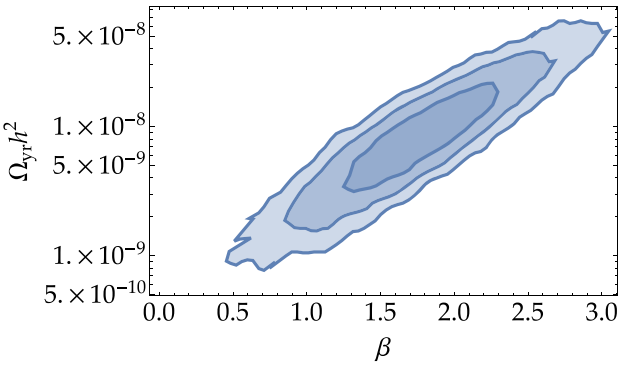

FIG. 3. The NANOGrav 15-year constraint $(1/2/3\sigma)$ on the amplitude $\Omega_{\mathrm{yr}}h^2$ and the power β for the power-law assumption $\Omega_{\mathrm{GW}}h^2(f) = \Omega_{\mathrm{yr}}h^2(f/f_{\mathrm{yr}^{-1}})^\beta$ (see Eq. (13) for the definition of the GW density parameter $\Omega_{\mathrm{GW}}h^2$), translated from Fig. 11 of Ref. [1].

$$\hat{\Phi}_{\mathbf{k}}''(\eta) + 3\mathcal{H}(1+c_s^2)\hat{\Phi}_{\mathbf{k}}'(\eta) + \left[c_s^2 k^2 + 3\mathcal{H}^2(c_s^2 - w)\right]\hat{\Phi}_{\mathbf{k}}(\eta) = 0. \quad (3)$$

Here $\hat{\Phi}_{\mathbf{k}}(\eta)$ is decomposed into the transfer function $\Phi_k(\eta)$ and the primordial perturbation $\hat{\psi}_{\mathbf{k}}$ as $\hat{\Phi}_{\mathbf{k}}(\eta) = \Phi_k(\eta)\hat{\psi}_{\mathbf{k}}$. $\hat{\psi}_{\mathbf{k}}$ is related to the gauge-invariant curvature perturbation $\hat{\zeta}_{\mathbf{k}}$ by $\hat{\psi}_{\mathbf{k}} = -2\hat{\zeta}_{\mathbf{k}}/3$ and the initial condition of the transfer function is given by $\Phi_k(\eta) \to 1$ and $\Phi_k'(\eta) \to 0$ for $\eta \to 0$.

The second-order effect of $\hat{\Phi}_{\mathbf{k}}(\eta)$ can source the linear tensor perturbation $\hat{h}_{\mathbf{k}}(\eta)$ through the equation,

$$\Lambda_\eta\left(a(\eta)\hat{h}_{\mathbf{k}}(\eta)\right) = 4a(\eta)\hat{\mathcal{S}}_{\mathbf{k}}(\eta), \quad (4)$$

where Λ_η is the derivative operator

$$\Lambda_\eta = \partial_\eta^2 + k^2 - \frac{1-3w(\eta)}{2}\mathcal{H}^2(\eta), \quad (5)$$

and $\hat{\mathcal{S}}_{\mathbf{k}}(\eta)$ represents the source term

$$\hat{\mathcal{S}}_{\mathbf{k}}(\eta) = \int \frac{d^3\tilde{\mathbf{k}}}{(2\pi)^3} e_{ij}(\mathbf{k})\tilde{k}^i\tilde{k}^j\left[2\hat{\Phi}_{\tilde{\mathbf{k}}}(\eta)\hat{\Phi}_{\mathbf{k}-\tilde{\mathbf{k}}}(\eta) + \frac{4}{3(1+w(\eta))}\left(\hat{\Phi}_{\tilde{\mathbf{k}}}(\eta) + \frac{\hat{\Phi}_{\tilde{\mathbf{k}}}'(\eta)}{\mathcal{H}(\eta)}\right)\left(\hat{\Phi}_{\mathbf{k}-\tilde{\mathbf{k}}}(\eta) + \frac{\hat{\Phi}_{\mathbf{k}-\tilde{\mathbf{k}}}'(\eta)}{\mathcal{H}(\eta)}\right)\right]. \quad (6)$$

$e_{ij}(\mathbf{k})$ is one polarization tensor. This sourced equation can be solved in the Green's function method as

$$\hat{h}_{\mathbf{k}}(\eta) = \frac{4}{a(\eta)}\int d\tilde{\eta} G_k(\eta,\tilde{\eta})[a(\tilde{\eta})\hat{\mathcal{S}}_{\mathbf{k}}(\tilde{\eta})], \quad (7)$$

with the Green's function $G_k(\eta,\tilde{\eta})$:

$$\Lambda_\eta G_k(\eta,\tilde{\eta}) = \delta(\eta-\tilde{\eta}). \quad (8)$$

Practically, the Green's function can be constructed by the two independent homogeneous solutions, $\Lambda_\eta g_{1k}(\eta) = \Lambda_\eta g_{2k}(\eta) = 0$, as

$$G_k(\eta,\tilde{\eta}) = \frac{g_{1k}(\eta)g_{2k}(\tilde{\eta}) - g_{1k}(\tilde{\eta})g_{2k}(\eta)}{g_{1k}'(\tilde{\eta})g_{2k}(\tilde{\eta}) - g_{1k}(\tilde{\eta})g_{2k}'(\tilde{\eta})}\Theta(\eta-\tilde{\eta}). \quad (9)$$

Eventually, the GW power spectrum is given by

$$\mathcal{P}_h(k,\eta) = \frac{64}{81a^2(\eta)}\int_{|k_1-k_2|\le k\le k_1+k_2} d\ln k_1 d\ln k_2 I^2(k,k_1,k_2,\eta)\frac{(k_1^2 - (k^2-k_2^2+k_1^2)^2/(4k^2))^2}{k_1k_2k^2}\mathcal{P}_\zeta(k_1)\mathcal{P}_\zeta(k_2), \quad (10)$$

where

$$I(k,k_1,k_2,\eta) = k^2\int_0^\eta d\tilde{\eta} a(\tilde{\eta})G_k(\eta,\tilde{\eta})\left[2\Phi_{k_1}(\tilde{\eta})\Phi_{k_2}(\tilde{\eta}) + \frac{4}{3(1+w(\tilde{\eta}))}\left(\Phi_{k_1}(\tilde{\eta}) + \frac{\Phi_{k_1}'(\tilde{\eta})}{\mathcal{H}(\tilde{\eta})}\right)\left(\Phi_{k_2}(\tilde{\eta}) + \frac{\Phi_{k_2}'(\tilde{\eta})}{\mathcal{H}(\tilde{\eta})}\right)\right]. \quad (11)$$

The GW density parameter is well approximated by its oscillation average $\overline{\mathcal{P}_h(k,\eta)}$ well after its horizon reentry as

$$\Omega_{\rm GW}(k,\eta) = \frac{\rho_{\rm GW}(\eta,k)}{3M_{\rm Pl}^2H^2} = \frac{1}{24}\left(\frac{k}{\mathcal{H}}\right)^2\overline{\mathcal{P}_h(k,\eta)}, \quad (12)$$

where $H = \mathcal{H}/a$ is the ordinary Hubble parameter. It is extended to the current time η_0 with the current radiation density parameter $\Omega_{r0}h^2 = 4.2\times10^{-5}$ as

$$\Omega_{\rm GW}(k,\eta_0)h^2 = \Omega_{r0}h^2\left(\frac{a_c\mathcal{H}_c}{a_f\mathcal{H}_f}\right)^2\frac{1}{24}\left(\frac{k}{\mathcal{H}_c}\right)^2\overline{\mathcal{P}_h(k,\eta_c)}, \quad (13)$$

where $h = H_0/(100\ \mathrm{km\,s^{-1}\,Mpc^{-1}})$ is the normalized Hubble constant, the subscripts "c" and "f" indicate the time when the GW of interest becomes well subhorizon and the density parameter becomes almost constant (to which time we solve the induced GW) and the time when all relevant phase transitions are completed and g_* and g_{*s} well asymptote to the current values (to which time we solve the background dynamics).

In this way, the induced GWs can be calculated on an arbitrary background. In Fig. 2, we show the example GW spectrum normalized by the scalar amplitude squared A_ζ^2 for the scale-invariant scalar perturbation $\mathcal{P}_\zeta(k) = A_\zeta$.

Gravitational wave signals. We then calculate the GW spectrum, particularly in the NANOGrav's sensitivity range $f = 2$–59 nHz for the (compact) power-law-type power spectrum of the curvature perturbation[2]:

[2]Do not confuse this n_s with the inferred value $n_s = 0.965 \pm 0.004$ by the cosmic microwave background (CMB) observation [32]. They correspond to different perturbation scales and are independent of each other in principle.

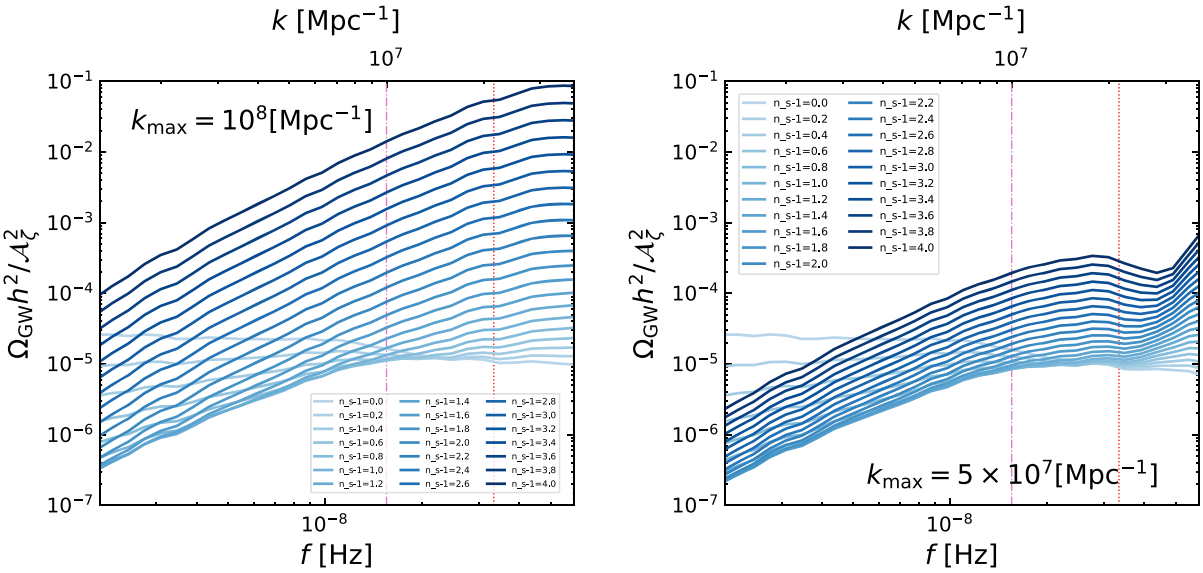

FIG. 4. Resultant GW spectra with $k_{\rm max} = 10^8$ Mpc^{-1} (left) or $k_{\rm max} = 5 \times 10^7$ Mpc^{-1} (right) for various values of the spectral index $n_{\rm s}$ within the NANOGrav's sensitivity range $f = 2$–59 nHz. The vertical red dotted line shows the pivot scale $f_{\rm yr^{-1}}$ and the vertical pink dot-dashed line represents $k = 10^7$ Mpc^{-1} below which the spectrum is fitted by the power-law function (15).

$$\mathcal{P}_\zeta(k) = A_\zeta \left(\frac{k}{k_{\rm yr^{-1}}}\right)^{n_{\rm s}-1} \Theta(k - k_{\rm min})\Theta(k_{\rm max} - k), \quad (14)$$

where $k_{\rm yr^{-1}} = 2\pi \times 1$ yr^{-1} $\simeq 2 \times 10^7$ Mpc^{-1} is the pivot scale and we restrict perturbations to a certain range $k_{\rm min} \le k \le k_{\rm max}$. In particular, since NANOGrav's data favor the blue-tilted spectrum, the upper bound $k_{\rm max}$ is practically necessary for the power spectrum not to exceed the unity and break the perturbativity. We take $k_{\rm max} = 10^8$ Mpc^{-1} as a fiducial value but the GW spectrum can be sensitive to $k_{\rm max}$ and we will also show the result for $k_{\rm max} = 5 \times 10^7$ Mpc^{-1} as a comparison. $k_{\rm min}$ is irrelevant in our setup and fixed to $k_{\rm min} = 10^5$ Mpc^{-1}. In Fig. 4, the resultant GW spectra normalized by A_ζ^2 are shown for several values of $n_{\rm s}$. Particularly in the low-frequency range to which pulsar timing array experiments are sensitive, they can be fitted by a power-law function

$$\Omega_{\rm GW}(f)h^2 \approx Q(x)A_\zeta^2 \left(\frac{f}{f_{\rm yr^{-1}}}\right)^{\beta(x)}, \quad (15)$$

with $x \equiv n_{\rm s} - 1$ and the fitting parameters $Q(x)$ and $\beta(x)$. Figures 5 and 6 show fitting values of these parameters for each numerically-obtained GW spectrum, where we only used the data of $k \le 10^7$ Mpc^{-1} for better fitting. From this, one can further find the fitting formula for these fitting parameters themselves as

$$Q(x) \approx 10^a(1 + 10^{(bx+c-a)/d})^d,$$
$$\beta(x) \approx e\tanh(fx) - g, \quad (16)$$

where the fitting parameters a, b, c, d, e, f, g are summarized in Table I. We note that while the power β is given by an intuitive relation $\beta \sim 2(n_{\rm s} - 1)$ in the nearly-scale-invariant case, β shows a certain upper bound $\beta \lesssim 3$ for larger $n_{\rm s}$. In fact, it is known that for the broken-power-law primordial power spectrum, the low-frequency tail of GWs asymptotes to $\propto k^3$ if $n_{\rm s} - 1 \ge 3/2$ [20,33]. Therefore, β cannot exceed three in our setup. We have also confirmed that our numerical scheme is consistent with the analytic formulas derived in Refs. [34,35] in the radiation-dominated universe.[3]

Making use of these formulae, the NANOGrav constraint on the GW spectrum with the power-law assumption shown in Fig. 3 can be interpreted as the constraint on the (compact) power-law-type primordial power spectrum as shown in Fig. 7. We also show the (mis)interpretation assuming the exact radiation background as a comparison. Additionally, we again stress the significance of imposing a practically required upper bound $k_{\rm max}$, on the power-law-type power spectrum. This constraint imposes an upper bound smaller than three on β. Consequently, the spectral index $n_{\rm s} - 1$ is not constrained from above in contrast to Fig. 19 of Ref. [6], where the limitations $k_{\rm min}$ and $k_{\rm max}$ are not put.

Summary and discussion. In this paper, we interpret the NANOGrav constraint on the GW spectrum (Fig. 3) in terms of the parameters for the power spectrum of the

[3]Some examples of the amplitude parameter $Q_{\rm RD}(n_{\rm s})$ (without the factor of $\Omega_{r0}h^2$) are shown in Table 1 of Ref. [35] but for the all integration range, $0 < k_1, k_2 < \infty$, in Eq. (10). The same analysis is done by the European Pulsar Timing Array collaboration [6].

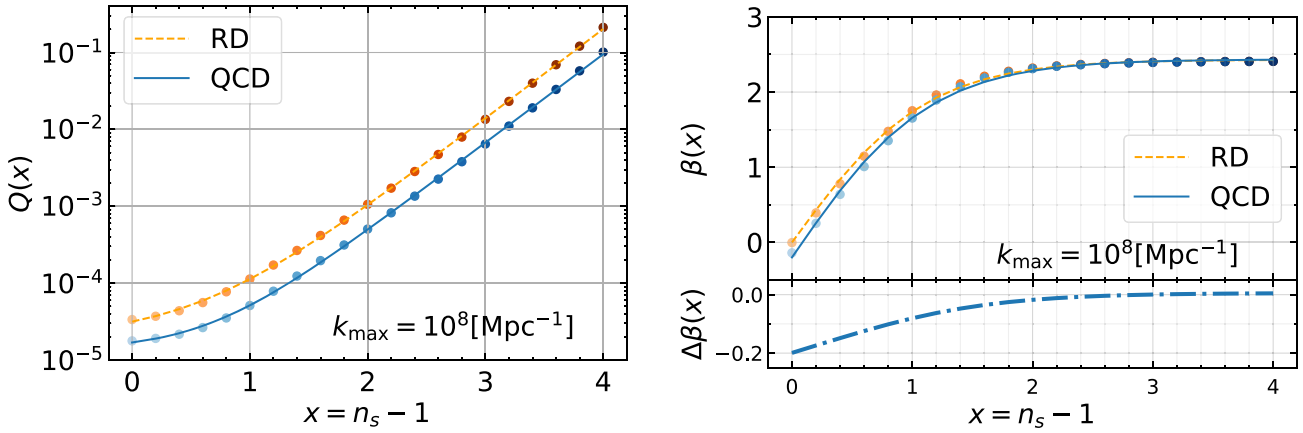

FIG. 5. Fitting parameters $Q(x)$ (left), $\beta(x)$ (right top) and the difference $\Delta\beta(x) = \beta_{\rm QCD}(x) - \beta_{\rm RD}(x)$ (right bottom) in the power-law fitting (15) for numerical results (points) and their own fitting formulae (16) (lines) for $k_{\rm max} = 10^8$ Mpc^{-1}. The blue ones are the results with the QCD effect while the orange ones are for the pure radiation-dominated universe as a comparison.

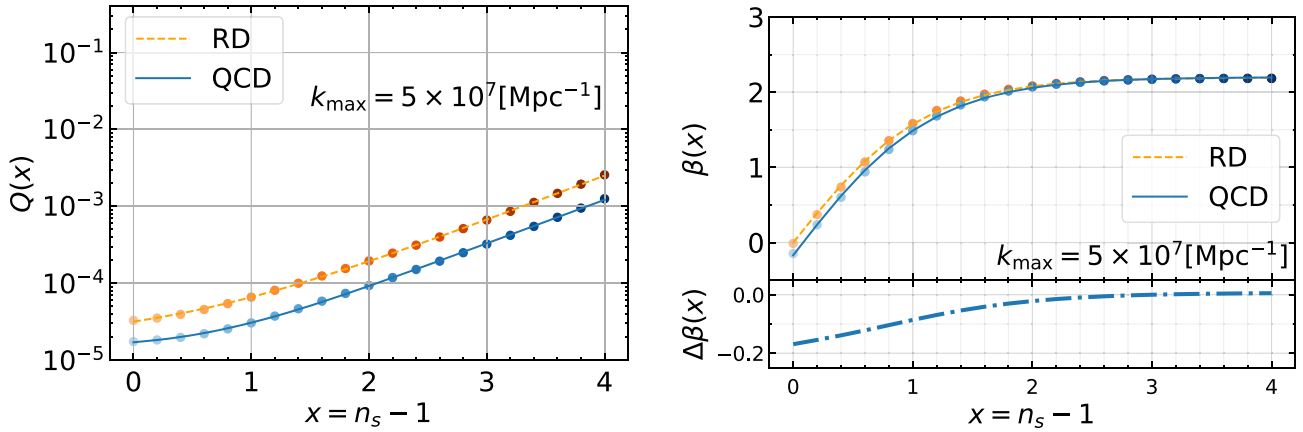

FIG. 6. Same as Fig. 5 but with $k_{\rm max} = 5 \times 10^7$ Mpc^{-1}.

primordial curvature perturbation (14), including the QCD phase-transition effect, as shown in Fig. 7. The constraint depends on the upper cutoff $k_{\rm max}$ in Eq. (14) and the spectral index is not constrained from above, which is because the GW spectrum with the power around or larger than three cannot be realized by the induced GWs from the broken-power-law primordial perturbation [20,33]. However, one finds that anyway neglecting the QCD effect would underestimate the amplitude of the primordial perturbation by about 25%. The spectral index could also be underestimated by up to 10% when $0 < n_{\rm s} - 1 < 1$ if one neglects the QCD effect.

We close the section by mentioning the implication of our result on the PBH formation. The PBH formation is also affected by the QCD phase transition (see, e.g., Refs. [36–38] and also Refs. [39,40] for detailed numerical studies on this effect) and the corresponding scenario is sometimes referred to as the *thermal history* model [41,42]. Reference [43] claims that this thermal history model is consistent with several observational "positive evidence" of PBHs (see also the review article [44]). Nevertheless, these works basically focused on the almost scale-invariant case $n_{\rm s} \simeq 0.96$ and cannot be directly applied to our spectrum $n_{\rm s} - 1 \sim 1$ inferred by the NANOGrav data. Just regarding

TABLE I. Fitting parameters in Eq. (16) for the amplitude $Q(x)$ and the power $\beta(x)$ shown in Figs. 5 and 6.

$k_{\rm max}$	Background	a	b	c	d	e	f	g
10^8 Mpc^{-1}	QCD	−4.854	1.139	−5.593	1.068	2.636	0.8752	0.1983
	RD	−4.684	1.155	−5.328	1.420	2.431	0.8975	0
5×10^7 Mpc^{-1}	QCD	−4.829	0.5616	−5.170	0.6002	2.370	0.8648	0.1686
	RD	−4.702	0.5718	−4.899	0.9659	2.194	0.9020	0

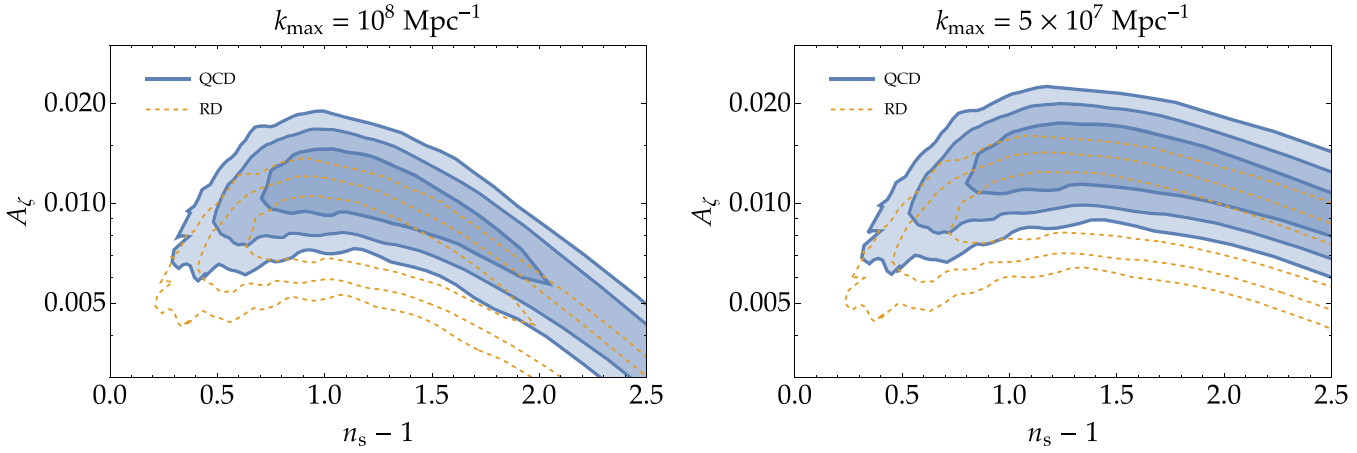

FIG. 7. The inferred parameter region of the primordial power spectrum by the latest NANOGrav data (Fig. 11 of Ref. [1]) with (blue) and without (orange-dashed) the QCD effect.

the amplitude, Ref. [43] supposes that the root-mean-square of the density contrast is $\sigma_\delta = 0.0218$ on the solar-mass scale. σ_δ coarse-grained on a scale R is related to the primordial power spectrum by (see, e.g., Ref. [19])

$$\sigma_\delta^2 = \frac{16}{81}\int \frac{{\rm d}k}{k} W^2(kR)(kR)^4 \mathcal{P}_\zeta(k), \tag{17}$$

and for the compact power-law power spectrum $\mathcal{P}_\zeta = A_\zeta (k/k_*)^{n_{\rm s}-1}\Theta(k-k_{\rm min})\Theta(k_{\rm max}-k)$ and the Gaussian window function $W(z) = {\rm e}^{-z^2/2}$, it is simplified as

$$\sigma_{\delta,{\rm PG}}^2 = \frac{8}{81} A_\zeta (k_* R)^{1-n_{\rm s}} \times \left[\Gamma\left(\frac{n_{\rm s}+3}{2}, k_{\rm min}^2 R^2\right) - \Gamma\left(\frac{n_{\rm s}+3}{2}, k_{\rm max}^2 R^2\right)\right], \tag{18}$$

where $\Gamma(a,x) = \int_x^\infty t^{a-1}{\rm e}^{-t}{\rm d}t$ is the incomplete gamma function. Making use of the mass-scale relation (see, e.g., Ref. [45])

$$M(R) \simeq 10^{20}\ {\rm g}\left(\frac{g_*(R)}{106.75}\right)^{-1/6}\left(\frac{R}{6.4\times 10^{-14}\ {\rm Mpc}}\right)^2, \tag{19}$$

one finds that the inferred value, $A_\zeta \sim 0.01$ and $n_{\rm s} - 1 \sim 1$ with $k_* = k_{\rm yr^{-1}}$, $k_{\rm min} = 10^5$ Mpc^{-1}, and $k_{\rm max} = 10^8$ Mpc^{-1} or 5×10^7 Mpc^{-1}, corresponds to $\sigma_{\delta,{\rm PG}} \sim 0.015$ on the solar-mass scale, which could be consistent with Ref. [43]. Detailed numerical studies for $n_{\rm s} - 1 \sim 1$ are anyway necessary.

Acknowledgments. Y. T. is supported by JSPS KAKENHI Grant No. JP21K13918.

[1] G. Agazie *et al.* (NANOGrav Collaboration), The NANOGrav 15-year data set: Evidence for a gravitational-wave background, Astrophys. J. Lett. **951**, L8 (2023).
[2] J. Antoniadis *et al.*, The second data release from the European Pulsar Timing Array III. Search for gravitational wave signals, Astron. Astrophys. **678**, A50 (2023).
[3] D. J. Reardon *et al.*, Search for an isotropic gravitational-wave background with the Parkes Pulsar Timing Array, Astrophys. J. Lett. **951**, L6 (2023).
[4] H. Xu *et al.*, Searching for the nano-hertz stochastic gravitational wave background with the Chinese Pulsar Timing Array data release I, Res. Astron. Astrophys. **23**, 075024 (2023).
[5] A. Afzal *et al.* (NANOGrav Collaboration), The NANOGrav 15 yr data set: Search for signals from new physics, Astrophys. J. Lett. **951**, L11 (2023).
[6] J. Antoniadis *et al.*, The second data release from the European Pulsar Timing Array: V. Implications for massive black holes, dark matter and the early Universe, arXiv:2306.16227.
[7] K. Tomita, Non-linear theory of gravitational instability in the expanding universe, Prog. Theor. Phys. **37**, 831 (1967).
[8] S. Matarrese, O. Pantano, and D. Saez, A general relativistic approach to the nonlinear evolution of collisionless matter, Phys. Rev. D **47**, 1311 (1993).

[9] S. Matarrese, O. Pantano, and D. Saez, General relativistic dynamics of irrotational dust: Cosmological implications, Phys. Rev. Lett. **72**, 320 (1994).
[10] S. Matarrese, S. Mollerach, and M. Bruni, Second order perturbations of the Einstein-de Sitter universe, Phys. Rev. D **58**, 043504 (1998).
[11] C. Carbone and S. Matarrese, A unified treatment of cosmological perturbations from super-horizon to small scales, Phys. Rev. D **71**, 043508 (2005).
[12] K. N. Ananda, C. Clarkson, and D. Wands, The cosmological gravitational wave background from primordial density perturbations, Phys. Rev. D **75**, 123518 (2007).
[13] D. Baumann, P. J. Steinhardt, K. Takahashi, and K. Ichiki, Gravitational wave spectrum induced by primordial scalar perturbations, Phys. Rev. D **76**, 084019 (2007).
[14] Z.-C. Chen, C. Yuan, and Q.-G. Huang, Pulsar Timing Array constraints on primordial black holes with NANOGrav 11-year dataset, Phys. Rev. Lett. **124**, 251101 (2020).
[15] R. Saito and J. Yokoyama, Gravitational wave background as a probe of the primordial black hole abundance, Phys. Rev. Lett. **102**, 161101 (2009); **107**, 069901(E) (2011).
[16] E. Bugaev and P. Klimai, Induced gravitational wave background and primordial black holes, Phys. Rev. D **81**, 023517 (2010).
[17] R. Saito and J. Yokoyama, Gravitational-wave constraints on the abundance of primordial black holes, Prog. Theor. Phys. **123**, 867 (2010).
[18] E. Bugaev and P. Klimai, Constraints on the induced gravitational wave background from primordial black holes, Phys. Rev. D **83**, 083521 (2011).
[19] K. Inomata, M. Kawasaki, K. Mukaida, Y. Tada, and T. T. Yanagida, Inflationary primordial black holes for the LIGO gravitational wave events and pulsar timing array experiments, Phys. Rev. D **95**, 123510 (2017).
[20] G. Domènech, Scalar induced gravitational waves review, Universe **7**, 398 (2021).
[21] S. Bird, I. Cholis, J. B. Muñoz, Y. Ali-Haïmoud, M. Kamionkowski, E. D. Kovetz, A. Raccanelli, and A. G. Riess, Did LIGO detect dark matter?, Phys. Rev. Lett. **116**, 201301 (2016).
[22] S. Clesse and J. García-Bellido, The clustering of massive primordial black holes as dark matter: Measuring their mass distribution with Advanced LIGO, Phys. Dark Universe **15**, 142 (2017).
[23] M. Sasaki, T. Suyama, T. Tanaka, and S. Yokoyama, Primordial black hole scenario for the gravitational-wave event GW150914, Phys. Rev. Lett. **117**, 061101 (2016); **121**, 059901(E) (2018).
[24] M. Sasaki, T. Suyama, T. Tanaka, and S. Yokoyama, Primordial black holes—perspectives in gravitational wave astronomy, Classical Quantum Gravity **35**, 063001 (2018).
[25] K. T. Abe, Y. Tada, and I. Ueda, Induced gravitational waves as a cosmological probe of the sound speed during the QCD phase transition, J. Cosmol. Astropart. Phys. 06 (2021) 048.
[26] K. Inomata, K. Kohri, and T. Terada, The detected stochastic gravitational waves and sub-solar primordial black holes, arXiv:2306.17834.
[27] Y.-F. Cai, X.-C. He, X. Ma, S.-F. Yan, and G.-W. Yuan, Limits on scalar-induced gravitational waves from the stochastic background by pulsar timing array observations, arXiv:2306.17822.
[28] S. Wang, Z.-C. Zhao, J.-P. Li, and Q.-H. Zhu, Exploring the implications of 2023 Pulsar Timing Array datasets for scalar-induced gravitational waves and primordial black holes, arXiv:2307.00572.
[29] L. Liu, Z.-C. Chen, and Q.-G. Huang, Implications for the non-Gaussianity of curvature perturbation from Pulsar Timing Arrays, arXiv:2307.01102.
[30] G. Franciolini, D. Racco, and F. Rompineve, Footprints of the QCD crossover on cosmological gravitational waves at Pulsar Timing Arrays, arXiv:2306.17136.
[31] K. Saikawa and S. Shirai, Primordial gravitational waves, precisely: The role of thermodynamics in the standard model, J. Cosmol. Astropart. Phys. 05 (2018) 035.
[32] N. Aghanim *et al.* (Planck Collaboration), Planck 2018 results. VI. Cosmological parameters, Astron. Astrophys. **641**, A6 (2020); **652**, C4(E) (2021).
[33] V. Atal and G. Domènech, Probing non-Gaussianities with the high frequency tail of induced gravitational waves, J. Cosmol. Astropart. Phys. 06 (2021) 001.
[34] J. R. Espinosa, D. Racco, and A. Riotto, A cosmological signature of the SM Higgs instability: Gravitational waves, J. Cosmol. Astropart. Phys. 09 (2018) 012.
[35] K. Kohri and T. Terada, Semianalytic calculation of gravitational wave spectrum nonlinearly induced from primordial curvature perturbations, Phys. Rev. D **97**, 123532 (2018).
[36] K. Jedamzik, Primordial black hole formation during the QCD epoch, Phys. Rev. D **55**, R5871 (1997).
[37] C. T. Byrnes, M. Hindmarsh, S. Young, and M. R. S. Hawkins, Primordial black holes with an accurate QCD equation of state, J. Cosmol. Astropart. Phys. 08 (2018) 041.
[38] K. Jedamzik, Consistency of primordial black hole dark matter with LIGO/Virgo merger rates, Phys. Rev. Lett. **126**, 051302 (2021).
[39] A. Escrivà, E. Bagui, and S. Clesse, Simulations of PBH formation at the QCD epoch and comparison with the GWTC-3 catalog, J. Cosmol. Astropart. Phys. 05 (2023) 004.
[40] I. Musco, K. Jedamzik, and S. Young, Primordial black hole formation during the QCD phase transition: Threshold, mass distribution and abundance, arXiv:2303.07980.
[41] B. Carr, S. Clesse, J. García-Bellido, and F. Kühnel, Cosmic conundra explained by thermal history and primordial black holes, Phys. Dark Universe **31**, 100755 (2021).
[42] S. Clesse and J. Garcia-Bellido, GW190425, GW190521 and GW190814: Three candidate mergers of primordial black holes from the QCD epoch, Phys. Dark Universe **38**, 101111 (2022).
[43] B. Carr, S. Clesse, J. Garcia-Bellido, M. Hawkins, and F. Kuhnel, Observational evidence for primordial black holes: A positivist perspective, arXiv:2306.03903.
[44] A. Escrivà, F. Kuhnel, and Y. Tada, Primordial black holes, arXiv:2211.05767.
[45] Y. Tada and S. Yokoyama, Primordial black hole tower: Dark matter, earth-mass, and LIGO black holes, Phys. Rev. D **100**, 023537 (2019).